ELSEVIER

Journal of Nuclear Materials 277 (2000) 231–238

journal of nuclear materials

www.elsevier.nl/locate/jnucmat

An alternative explanation for evidence that xenon depletion, pore formation, and grain subdivision begin at different local burnups☆

J. Rest*, G.L. Hofman

Argonne National Laboratory, Energy Technology-212, 9700 S. Cass Avenue, Argonne, IL 60439, USA

Received 21 December 1998; accepted 16 July 1999

Abstract

In order to interpret the recent observation that xenon depletion, pore formation, and grain subdivision occur successively at increasing local burnups, a rate-theory-based model is used to investigate the nucleation and growth of cavities during low-temperature irradiation of UO_2 in the presence of irradiation-induced interstitial-loop formation and growth. Consolidation of the dislocation structure takes into account the generation of forest dislocations and capture of interstitial dislocation loops. The loops accumulate and ultimately evolve into a low-energy cellular dislocation structure. The cell walls have been previously identified as recrystallization nuclei. The calculations indicate that nanometer-size bubbles are associated with this cellular dislocation structure while the observed micron-size bubbles are presumed to be either preexisting pores deformed by adjacent grains and/or new pores formed in the new recrystallized grain-boundary junctions. Subsequent to recrystallization, gas released from the recrystallized grains feeds the preexisting pores and the recrystallized grains may appear to form a preferential concentration of subdivided grains around the growing pores. This picture is illustrated in a sequence of photomicrographs of irradiated U_3O_8.

1. Introduction

In a recent paper, Spino et al. [1] described experimental evidence that xenon depletion, pore formation, and grain subdivision occur successively at increasing local burnups. The rim region of high-burnup fuels is characterized by an exponential growth of porosity towards the pellet edge: a narrow band of fully recrystallized porous material exists at the pellet periphery, and a rather wide adjacent transition zone with partially recrystallized porous areas appears dispersed within the original matrix structure. The pores become more separated from each other toward the pellet interior, and Spino et al. [2] observed local-recrystallized regions around large pores (≈1.0–1.5 μm), extending a few submicrometers from the pore surface. For this reason, models for grain subdivision have been proposed that interpret the phenomenon as a consequence of the formation of pressurized gas bubbles via a loop-punching mechanism [2,3]. However, it is difficult to account for bubbles of the size observed to be sufficiently overpressurized in an irradiation environment. In the temperature range associated with rim formation (<773 K), estimates of bubble overpressure are more than a factor of 3 lower than that required for irradiation-induced creep of UO_2 [2]. Irradiation provides an overabundance of defects that work toward bubble equilibration. However, the presence of a cellular dislocation structure could facilitate recrystallization (grain subdivision) by the mechanism proposed by Rest and Hofman [4] and observed by Ray et al. [5] and by Nogita and Une [6]. In the model proposed by Rest and Hofman, impurities that form during fissioning of the material diffuse as vacancy-impurity complexes to cell walls, where they

☆ Work supported by US Department of Energy, Office of Arms Control and Nonproliferation, under Contract W-31-109-Eng-38.

* Corresponding author.

0022-3115/00/$ - see front matter
PII: S0022-3115(99)00201-9

effectively pin the wall, i.e., the movement of the wall is hindered. Not all cell walls are uniformly affected by impurities; the walls containing no impurities continue to undergo subgrain coalescence that results in viable nuclei for recrystallization. Recrystallization is induced when the energy per nucleus is high enough that the creation of grain-boundary surfaces is offset by the creation of strain-free volumes, with a resultant net decrease in the free energy of the material. In the analysis presented here, one candidate for such an impurity is identified as a fission-gas atom.

The interstitial loops accumulate and ultimately evolve into a low-energy cellular dislocation structure. Previous calculations of the dislocation density (usually taken as the interstitial loop line length) have ignored these constraints on the growth of the loop size distribution [7–11]. To remedy these shortcomings, a coupled model for the calculation of the dislocation density and cavity-size distribution in UO_2 is presented below.

2. Matrix model

The model consists of a set of coupled equations for the time rate of change of the vacancy (c_v) and interstitial (c_i) concentrations, the interstitial loop diameter (d_l) and density (n_l), the density of forest dislocations (f_d), the cavity radius (r_c) and density (c_c), the average number of gas atoms in each cavity (N_g), and the concentration of gas atoms in solution in the fuel matrix (c_g). These equations are

$$\frac{dc_v(t)}{dt} = K - \alpha_r c_v(t)c_i(t) - k_v(\rho_l)D_v c_v(t) - 2\Omega^{1/3} b_v D_v c_v(t) n_l(t)/\pi d_l(t), \tag{1}$$

$$\frac{dc_i(t)}{dt} = K - \alpha_r c_v(t)c_i(t) - k_i(\rho_l)D_i c_i(t) - \sqrt{2} D_i c_i(t) c_i(t)/\Omega^{2/3} + 2\Omega^{1/3} b_v D_v c_v(t) n_l(t)/\pi d_l(t), \tag{2}$$

$$\frac{dn_l(t)}{dt} = \frac{\sqrt{2}}{2} D_i c_i(t) c_i(t)/\Omega^{5/3} - 4 v_l(t) n_l/d_l(t) - 2\Omega^{-2/3} b_v D_v c_v(t) n_l(t)/\pi d_l(t), \tag{3}$$

$$\frac{dd_l(t)}{dt} = g(t)\left(v_l(t) - (d_l(t) - d_0)\frac{n_l'(t)}{n_l(t)}\right), \tag{4}$$

$$\frac{df_d(t)}{dt} = \frac{d(\pi n_l(t) d_l(t))}{dt}, \tag{5}$$

$$\frac{dr_c(t)}{dt} = k_v(\rho_l) D_v \left(c_v(t) - c_v^0(t)\right) - k_i(\rho_l) D_i c_i(t), \tag{6}$$

$$\frac{dc_g(t)}{dt} = G - 16\pi f_n r_g D_g c_g(t) c_g(t) - 4\pi D_g r_c(t) c_c(t) c_g(t) + b N_g(t) c_c(t) - \frac{6}{d_g} \frac{D_g \partial c_g(x,t)}{\partial r}\bigg|_{r=d_g/2}, \tag{7}$$

$$\frac{dc_c(t)}{dt} = 16\pi f_n r_g D_g c_g(t) c_g(t)/N_g(t) - 16\pi D_c c_c(t) c_c(t)), \tag{8}$$

$$\frac{dN_g(t)}{dt} = 4\pi r_c D_g c_g(t) - b N_g(t) + 16\pi D_c N_g(t) r_c(t) c_c(t), \tag{9}$$

where

$$c_v^0(t) = c_v^T e^{-\left(P_g - 2\gamma/r_c(t) - \sigma\right)/\Omega kT}, \tag{10}$$

$$v_l(t) = \frac{2}{b_v}(z_i D_i c_i(t) - z_v D_v c_v(t)), \tag{11}$$

and

$$\rho(t) = \rho_l(t) + f_d(t), \tag{12}$$

where

$$\rho_l(t) = \pi n_l(t) d_l(t). \tag{13}$$

In the above equations, K is the damage rate in dpa/s; α_r is the recombination coefficient (discussed below); $b_v = \frac{1}{2} a\langle 1\,1\,0\rangle$ and Ω are the Burgers vector and atomic volume, respectively, where a is the lattice constant ($a = 5.47 \times 10^{-10}$ m); D_v, D_i, and D_g are the vacancy, interstitial, and gas-atom diffusivities, respectively; $k_v(\rho_l)$ and $k_i(\rho_l)$ are the vacancy and interstitial sink strengths [12]; f_n is the gas bubble nucleation factor; b is the gas-atom re-solution rate from bubbles; r_g is the gas-atom radius; G is the gas-atom generation rate in atoms/cm^3/s; z_v and z_i are the vacancy and interstitial bias factors; c_v^T is the thermal equilibrium vacancy concentration; P_g is the internal gas pressure in the cavity; σ is the external stress on the cavity (assumed = 0); d_g is the grain diameter; and γ is the surface energy. The fourth term on the right-hand side (RHS) of Eq. (2) and the first term on the RHS of Eq. (3) represent the nucleation of loops by di-interstitials; the last terms on the RHS of Eqs. (1)–(3) represent the loss of interstitial loops due to adsorption of vacancies; the first term on the RHS of Eq. (5) and the second term on the RHS of Eq. (3) represent the generation of forest dislocations by loops; the two terms on the RHS of Eq. (6) represent the change in radius of a cavity due to the influx of vacancies (growth) and interstitials (shrinkage), respectively; the last term on the RHS of Eq. (7) represents the diffusion of fission gas atoms to the grain boundaries. This term is estimated in a separate 2-D calculation that does not include the defect behavior equations. Loop growth is treated in a

straightforward manner. Instead of calculating loop size distribution, an average loop density, $n_l(t)$, and diameter, $d_l(t)$, is calculated by Eqs. (3) and (4), respectively. The first term on the RHS of Eq. (4) is the net growth rate of existing loops, which is the difference between the growth by absorbing interstitials while emitting vacancies and the shrinkage by absorbing vacancies. The second term is the change of the average diameter due to the formation of new loops (di-interstitials) with diameter d_0 [11]. In Eqs. (1)–(4), direct defect cluster formation in the cascade has been neglected. In addition, annihilation of adjacent dislocations due to stress induced glide has been omitted from the RHS of Eq. (5).

The dislocation loops accumulate according to Eq. (3) and ultimately evolve into a low-energy cellular dislocation structure. It is assumed here that loop growth (Eq. (4)) continues until a cellular dislocation microstructure forms, i.e.,

$$g(t) = C_A C_\rho \sqrt{\frac{\pi}{f(v)}} - d_l(t)\sqrt{\rho_l(t)} = 0, \tag{14}$$

where $f(v) = ((1-v)/2)/(1-v)$, v is Poisson's ratio (0.31), $C_A = 3$ for cupic cells and C_ρ is within a factor of 2 or so either way of unity [13]. The condition given by Eq. (14) is obtained by minimization of the total energy (dislocation line energy plus the energy stored in isolated terminating dislocation boundaries). Once Eq. (14) is satisfied it is assumed that a stable cellular dislocation microstructure with a fixed cell size has been attained. In reality, the continued pileup of dislocations on the cell walls will result in a decrease in cell size in order to maintain the lowest energy configuration.

When Eq. (14) is satisfied, the loops can no longer grow (see Eq. (4)) and the interlocked loops form a cellular dislocation structure. The dislocations associated with forest dislocations, $f_d(t)$, are assumed to be located primarily on the walls of the cellular dislocation structure. Thus, $f_d(t)$ is absent from the defect sink terms $k_v(\rho_l)$ and $k_i(\rho_l)$. Once Eq. (14) is satisfied, interstitial loops and forest dislocations generated within the cells continue to accumulate on the cell walls and increase the angle of the wall evolving the cellular dislocation structure into a subgrain boundary structure. This picture of recrystallization will be treated in a future publication.

3. Matrix analysis

Eqs. (1)–(16) were solved numerically for a fission rate of 2×10^{13} fissions cm^{-3} s^{-1} and a fuel temperature of 1073 K. The vacancy and interstitial migration enthalpies, ε_{vm} and ε_{im}, respectively, and the dislocation bias factor for interstitials, z_i, are the more sensitive parameters in the theory for these operating conditions (low temperature).

The vacancy, interstitial, and gas-atom diffusivities are given by

$$D_v = x_i^2 a^2 \upsilon_v e^{-\varepsilon_{vm}/kT}, \tag{15}$$

$$D_i = \frac{2}{3} x_i^2 a^2 \upsilon_i e^{-\varepsilon_{im}/kT}, \tag{16}$$

and

$$D_g = D_g^T + D_0^I \dot{f}, \tag{17}$$

where $\dot{f}$ is the fission rate in fissions/cm^3/s, $\upsilon_v(5\times10^{13}\ s^{-1})$ and $\upsilon_i(5\times10^{12}\ s^{-1})$ are the vacancy and interstitial jump frequencies, respectively, and D_g^T is the thermal component of the gas-atom diffusivity. x_i $\left(x_i^2 = 0.025\right)$ is a factor that takes into account the deviation from stoichiometry. x_i^2 has been estimated to be in the range 10^{-2}–1 [14]. The irradiation-enhanced diffusion coefficient given by Eq. (17) with $D_0^I = 3.5\times10^{-30}$ cm^5 lies within the scatter of the measured diffusion coefficients in oxides, mixed oxides, carbides, and nitrides [15].

Ionic charge effects (not included in the rate theory model given by Eqs. (1)–(9) may be important in point defect recombination barriers/wells, etc. For an f.c.c. lattice, the reaction rate constant, α_r, for vacancy/interstitial recombination that appears in Eqs. (1) and (2), assuming that $D_v \ll D_i$, is given by [16]

$$\alpha_r = \frac{12}{x_i^2 a^2}\left(\frac{3}{2}D_i + D_v\right) \approx \frac{18 D_i}{x_i^2 a^2}. \tag{18}$$

α_r can also be expressed as [17]

$$\alpha_r = 4\pi r_{iv}(D_i + D_v)/\Omega \approx \frac{4\pi r_{iv} D_i}{\Omega}, \tag{19}$$

where r_{iv} is the radius of the recombination volume. Thus, comparing Eqs. (18) and (19)

$$r_{iv} \approx \frac{18\Omega}{4\pi\, x_i^2 a^2} = 8.25\ \times\ 10^{-9}\ \text{m}. \tag{20}$$

The value of the recombination volume given by Eq. (20) is $\approx 5\times10^4$ atomic volumes. The value of the recombination volume depends on x_i^2: larger values of x_i^2 result in smaller values of the recombination volume. For example, $x_i^2 = 1$ results in a value of the recombination volume given by Eq. (20) of $\approx$50 atomic volumes. This value is consistent with calculated estimates for copper [18], and with empirical (resistivity) estimates for copper and other fcc metals [19]. The calculated value of $\approx 5\times10^4$ atomic volumes is considered to be an effective recombination volume arising because of the effect of

stoichiometry due to charged defects in an ionic material (UO_2).

Some comments are in order on the use of a single-lattice theory model to analyze a two-sublattice material (UO_2). The value of ε_{vm} used in the calculations (2.4 eV) is the uranium vacancy migration enthalpy in UO_2 [15]. This is the appropriate rate-limiting (slower) point defect migration enthalpy for a single-sublattice rate theory model of UO_2. The nominal values used for the other parameters are $\varepsilon_{im} = 0.6$ eV and $z_i = 1.001$ ($z_v = 1$). ε_{im} is taken to be the uranium interstitial migration enthalpy in UO_2 and is assumed to be larger than that for the oxygen interstitial. Because of stoichiometry constraints, the uranium interstitial migration enthalpy is the appropriate rate limiting (slower) choice for this single-sublattice rate theory model of UO_2 [14,20].

Fig. 1 shows $d_l(t)\sqrt{\rho_l(t)}$ plotted as a function of fuel burnup for three values of z_i (Fig 1(a)), and three values of ε_{im} (Fig 1(b)). The nominal values of these parameters are $z_i = 1.001$ and $\varepsilon_{im} = 0.6$ eV. The calculations shown in Fig. 1 used a value of $C_A C_\rho \sqrt{\pi/(f(\upsilon))} = 5$ in Eq. (14). This is at the lower end of the range of values given in Ref. [13] for copper and aluminum. The results shown in Fig. 1 indicate that the transition from a fine dislocation loop structure to a cellular dislocation structure occurs earlier for larger values of z_i and ε_{im}. For the nominal values of these parameters ($z_i = 1.001, \varepsilon_{im} = 0.6$ eV), this transition occurs at ≈60 MWd/kg).

Fig. 2 shows the calculated total dislocation density as a function of burnup for three values of z_i (Fig. 2(a)), and three values of ε_{im} (Fig 2(b)). Also shown in Fig. 2 is the fit (over the range 6–44 MWd/kg) to the measured dislocation density [21]. The calculations shown in Fig. 2 indicate that the calculated dislocation density increases for larger values of z_i (Fig. 2) and larger values of ε_{im} (Fig. 2(b)). For the nominal values of these parameters ($z_i = 1.001, \varepsilon_{im} = 0.6$ eV), the calculated dislocation density is in reasonable agreement with the data at 44 MWd/kg. The trend of the calculations shows a linear behavior as compared to a parabolic behavior as demonstrated by the data. A reason for this discrepancy could be the absence in Eq. (5) of stress-induced glide and forest dislocation annihilation processes (such as annihilation of adjacent dislocations of opposite sign).

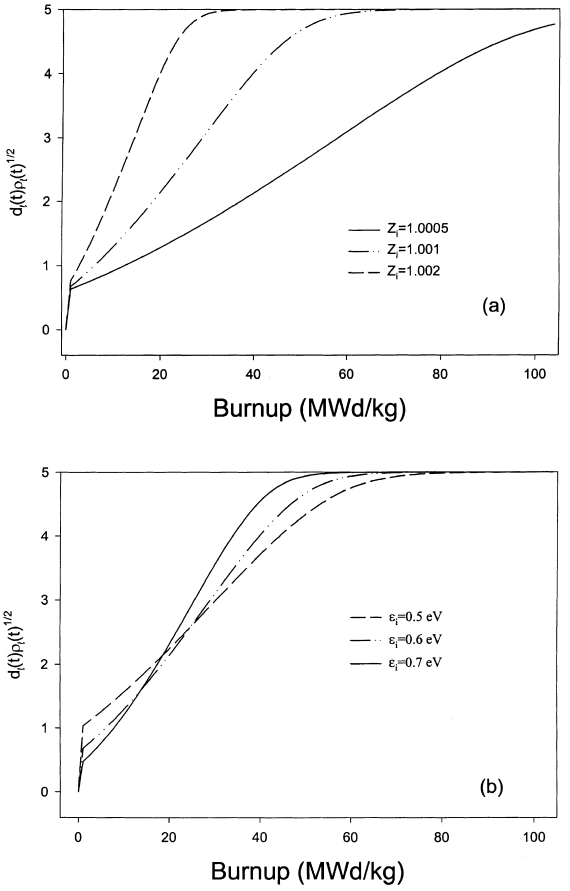

Fig. 1. $d_l(t)\sqrt{\rho_l(t)}$ as a function of burnup.

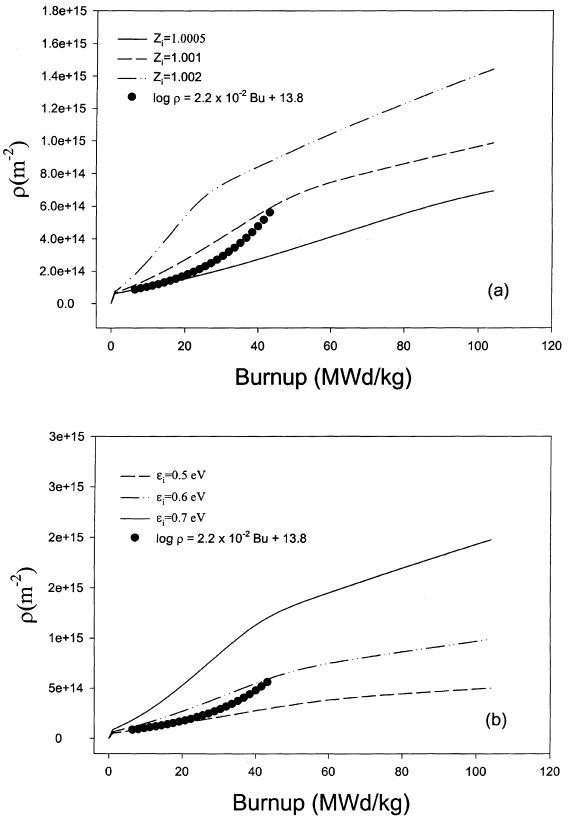

Fig. 2. Calculated total dislocation density $\rho = \rho_l + f_d$ as a function of burnup. Also shown is fit (over the range 6–44 MWd/kg) to measured dislocation density from Ref. [6].

The value of the dislocation bias factor used in the calculation of Figs. 1 and 2 is substantially smaller than values associated with the swelling of metals (usually in the range 1–10%). The very small bias (i.e., $z_i - z_v$) used in the present calculations for UO_2 is consistent with the apparent absence of void swelling in this material.

Fig. 3 shows the calculated interstitial-loop diameter and density as a function of burnup. The calculated total dislocation density increases rapidly early in the irradiation (due to nucleation of small dislocation loops) and then increases at an approximately linear rate as the loop population coarsens (see Fig. 3) and a dislocation network is generated. The loop density and diameter increase rapidly before reaching a saturation value at ≈ 60 MWd/kg. The results shown in Figs. 2 and 3 are in qualitative agreement with the behavior observed in Ref. [6] where dislocation loops were only visible at an intermediate burnup of $\approx$44 MWd/kg. Forest dislocations were present at all burnups between 20 and 80 MWd/kg. The total dislocation density (forest and loops) measured in Ref. [6] increase steadily with increasing burnup between 6 and 44 MWd/kg before reaching an apparent saturation level.

The cell size at steady state, i.e., when $d_l(t)\sqrt{\rho_l(t)} = 5$, is $\approx$300 nm. This is the predicted size of the cellular dislocation structure, or equivalently, the recrystallization nuclei, and, in the absence of grain growth, of the recrystallized grains. This value is consistent with those observed by Nogita and Une [6].

Fig. 4 shows the calculated intragranular bubble diameter and density as a function of burnup, compared with the measured quantities. The calculations shown in Fig. 4 were made with the value of the bubble nucleation factor $f_n = 1$, and the value for the gas-atom re-solution rate from bubbles $b = 0$. A key assumption of the gas-bubble distribution calculation shown in Fig. 4 is that the effects of irradiation-induced re-solution of fission-gas bubbles on subgrain boundaries are small because of the relatively strong sink-like property of the boundary.

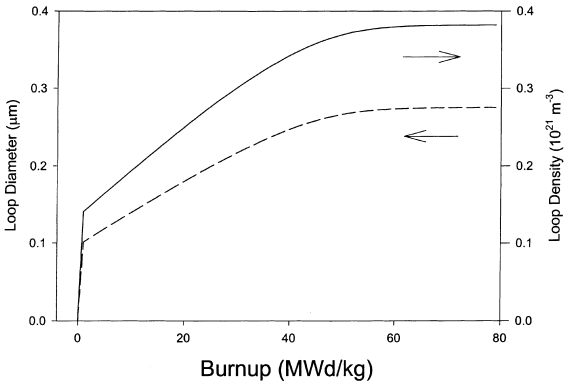

Fig. 3. Calculated interstitial-loop diameter and density as a function of burnup.

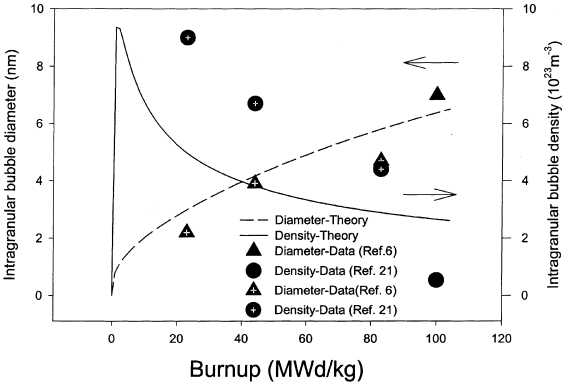

Fig. 4. Calculated intragranular bubble diameter and density as a function of burnup. Also shown are measured average bubble size (triangles) and number density (circles) from Refs. [6,21].

This assumption is generally accepted as valid for high-angle boundaries that result from fabrication processes [22]. The assumption made here for the subgrain boundaries is consistent with the observations reported in Refs. [6,21] that tangled dislocation networks with low-angle subgrain boundaries are formed by the inhomogeneous accumulation of dislocations.

The calculated bubble diameter (dashed line in Fig. 4) increases as a function of burnup and is consistent with the trend of observed intragranular bubble diameters (triangles in Fig. 4) reported in Refs. [6,21]. The calculated bubble density (solid line in Fig. 4) increases rapidly with burnup, peaks at $\approx$5 MWd/kg, and subsequently decreases with increasing burnup. This behavior follows the trend of the observed bubble density (circles in Fig. 4), which peaks early in the irradiation period and subsequently decreases with burnup. The reason for the decrease in the bubble density is bubble coarsening due to bubble–bubble interaction. The small bubbles on the cell walls are not calculated to contact each other due to geometrical considerations, but to interact due to surface diffusion processes. Decreasing the value of f_n decreases the height of the peak of the bubble density curve shown in Fig. 4 (for example reducing f_n to a value of 0.1 lowers the value of the peak from $\approx$8 to $\approx 2 \times 10^{23}$ m^{-3}). Increasing the value of b (for example to a value of 10^{-6}) totally eliminates the peak: the bubble density increases throughout the burnup range.

The interpretation given here that the observed nanometer-size bubbles are associated with the cellular (or subgrain) dislocation structure is consistent with observation. In particular, a subgrain structure is observed to begin forming in the fuel at a burnup between 30 and 44 MWd/kg [6]. The boundaries of this subgrain microstructure will act as a sink for fission gas and will deplete the intragranular gas density. Diffusion of gas to subgrain boundaries along with intergranular bubble interconnection is responsible for the loss of fission gas

from the fuel (i.e., xenon depletion). Subsequent to recrystallization, bubbles on the grain boundaries are calculated to interconnect (see Section 4).

The bubbles are calculated to be near or at equilibrium pressures. The lack of substantial overpressurization is due to the relatively high dislocation density (Fig. 2) that acts as a sink for interstitials. On the other hand, the lack of substantial bubble underpressurization is due to the relatively low bias used in the calculations. Interstitial depletion results in an enhanced vacancy concentration in the lattice. These excess vacancies are absorbed not only by dislocations, but also by intra and intergranular cavities.

4. Analysis of pore behavior in recrystallized fuel

Recall the observation made in Ref. [2] of pores having diameters of 1–1.5 μm that are surrounded with a preferential concentration of subdivided grains. The models for grain subdivision that have been proposed to interpret this phenomena as a consequence of the formation of pressurized gas bubbles via a loop punching mechanism are not supported by the above calculations, which indicate that the small intragranular bubbles are at or near equilibrium pressure. For these bubbles to be overpressurized (given the observed bubble-size distribution from Ref. [6]), a substantial decrease (one order of magnitude) in the observed dislocation density is estimated to be required. This is because a reduced dislocation density facilitates increased defect recombination, and a resultant reduction in vacancy availability for bubble relaxation. In addition, it is quite apparent from Fig. 4 that the calculated (and observed) bubble size is substantially below the bubble diameters observed in Ref. [2]. The conclusion reached here, therefore, is that the bubbles observed in Ref. [2] must have some preexisting origin, e.g., that is related to the as fabricated porosity or of intergranular nature, i.e., that have formed on recrystallized grain-boundary junctions. Sintered as-fabricated porosity has been observed to remain in UO_2 fuel at 23 MWd/kg [23]. However, recent TEM studies in as-fabricated UO_2 have demonstrated the presence of abundant submicron pores with highly strained surroundings, very similar to the rim pores, but without the associated grain subdivision [24]. A possibility exists that these kinds of pore, contributing only slightly to the total porosity because of their small size, survive in-pile densification. Thus, a significant number of these as-fabricated pores might survive irradiation so as to serve as precursors of the characteristic rim-pores observed at high burnups. In the prestrained regions near these micropores, the here- described dislocation cell formation could be preferentially initiated.

To assess the effect of recrystallization on the behavior of preexisting porosity, a calculation of bubble growth was performed with the GRASS-SST code [25]. The calculation takes into account fission gas behavior within the fuel matrix, diffusion to surfaces (e.g., grain boundaries), and bubble interaction on surfaces. Fig. 5 shows GRASS-SST calculated fission-gas-bubble-size distribution on recrystallized grain boundaries irradiated at 773 K to 66.6 MWd/kg. The grains are assumed to be spherical and to have a diameter of 0.3 μm. The calculations show that the intergranular bubble sizes are in the nanometer range. This is consistent with intergranular bubbles observed in recrystallized regions of UO_2 fuel (see Fig. 7 of Ref. [26]). Also, shown in Fig. 5 is the calculated pore diameter assuming a fixed density of preexisting pores (this density is taken from that derived from measured two-dimensional data of Refs. [1,2]). In the calculation, the gas feeding the pores is that released from the intergranular interconnected porosity in the recrystallized material surrounding the pores (the calculated fractional release at 66.6 MWd/kg is $\approx$ 10%). The calculated diameter of the preexisting pores is in the range of the measured average pore diameter data associated with local recrystallized zones from Ref. [2]. Thus, the calculations shown in Fig. 5 support the premise that the observed bubbles in Refs. [1,2] are either preexisting pores deformed by adjacent grains and/or new pores formed in the new recrystallized grain-boundary junctions.

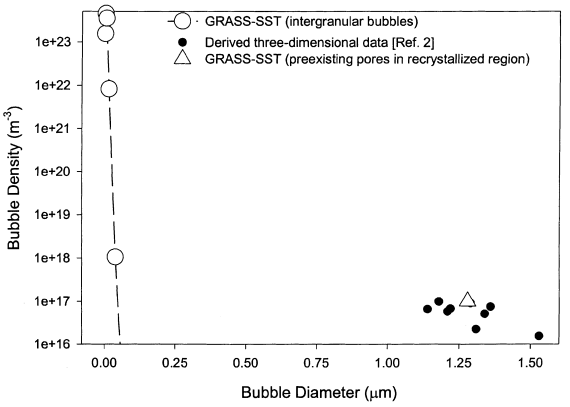

Fig. 5. GRASS-SST calculated fission-gas-bubble-size distribution on recrystallized grain boundaries (open circles) and for preexisting pores in the recrystallized region (solid triangle) at 66.6 MWd/kg. The average grain size and irradiation temperature used in the simulation was 0.3 μm and 773 K, respectively. Also shown are derived three-dimensional porosity data associated with local recrystallized zones from Ref. [2] (solid circles).

5. Supporting experimental observations

Prior to the discovery of the RIM effect in LWR high-burnup fuel, a very similar occurrence of grain-re-

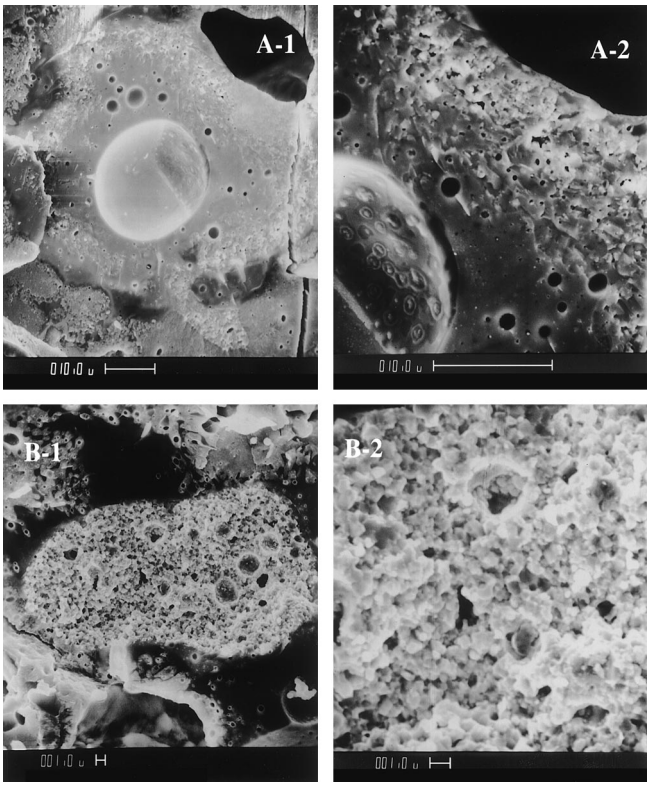

Fig. 6. Example of the microstructural changes in the center of uranium oxide–aluminum dispersion fuel particles irradiated to 80 (A-1) and (A-2) and 130 (B-1) and (B-2) MWd/kg burnup.

finement in uranium oxide–aluminum dispersion fuel was reported [27]. The fuel in this case consisted originally of U_3O_8 particles, but due to chemical interaction with the Al matrix the central part of the fuel particles was reduced to U_4O_9, a compound very similar to UO_2. An example of the microstructural changes in the center of these fuel particles is shown in Fig. 6. The similarity with SEM micrographs of the RIM in LWR fuel [28] is striking. The purpose of recalling this earlier study is to offer support for the premise of the present paper, i.e., gas bubbles are not the primary initiators of grain-refinement but rather a result thereof.

Fig. 6(A-1) shows the center of a fuel particle at approximately 80 MWd/kg burnup. Grain-refinement has occurred in some areas, (within the patchy regions). In these areas, small grains with diameters <0.5 μm can be observed. This agrees with the reported beginning of the RIM structure at a similar burnup [28]. The larger spherical pores in the unrestructured fuel, certainly the very large one in the center, are the remnants of original as-fabricated porosity. In contrast to observations reported in Ref. [2], recrystallized material surrounding these large pores is not apparent in Fig. 6(A-1). As shown in Fig. 6(A-2), these preexisting – to grain-refinement – pores do not appear to be preferentially associated with the grain-refined patches. The pores in the grain-refined structure are rather irregular in shape and, in the context of the present model, are either preexisting pores deformed by adjacent new grains and/or new pores formed in the new grain boundary junctions. At approximately 130 MWd/kg, as shown in Fig. 6(B-1), grain-refinement has occurred in total, the larger preexisting pores are incorporated in the new microstructure while, as shown in Fig. 6(B-2), smaller pores have developed heterogeneously on the refined grain boundary structure.

6. Conclusions

The relationship between xenon depletion, pore formation, and grain subdivision proposed in this paper is the result of the natural evolution of the fuel microstructure. Irradiation-induced interstitial-loop formation and growth generates forest dislocations. Consolidation of this dislocation structure in a lower-energy cellular pattern results in subgrain boundary formation. The formation of subgrain boundaries in the material provides short diffusion distances for the matrix gas. In addition, once the gas reaches the boundaries, intergranular

bubble dynamics lead to long-range porosity interconnections that provide pathways for fission-gas release to free surfaces. Thus, fission-gas release, or conversely Xe depletion, is initiated. Continued irradiation leads to the growth of intergranular bubbles on subgrain boundaries. Subsequently, irradiation-induced recrystallization occurs in the material surrounding the bubbles. The process of recrystallization provides additional driving forces for enhanced intergranular bubble growth (e.g., sweeping up of matrix gas, etc.). Gas released from the recrystallized material will feed preexisting pores (e.g., as-fabricated porosity). The recrystallized grains may appear to form a preferential concentration of subdivided grains around these pores [1]. This picture is illustrated in a sequence of photomicrographs of irradiated U_3O_8, and is counter to models of subgrain division (or oriented dislocation redistribution) that are based on matrix strain fields induced by the balance between pore gas inner pressure and external stress [29].

In previous work [4], cellular dislocation walls were postulated to be potential nuclei for recrystallization. The stored energy in the material is concentrated on the cell walls. The fraction of immobile walls increases with dose due to interaction with mobile, irradiation-produced impurities (i.e., vacancy–solute pairs). The above analysis suggests that a possible candidate for such an impurity is a fission-gas atom. This premise is supported by studies that suggest that fission gas diffuses in Schottky trios, trivacancies consisting of one U and two O vacancies [30]. Presumably, diffusive jumps of the gas atom are correlated with jumps of the slowest moving specie, the uranium vacancy.

Acknowledgements

The authors would like to thank J. Spino for interesting discussions.

References

[1] J. Spino, D. Baron, M. Coquerelle, A.D. Stalios, J. Nucl. Mater. 256 (1998) 189.
[2] J. Spino, K. Vennix, M. Coquerelle, J. Nucl. Mater. 231 (1996) 179.
[3] Hj. Matzke, J. Nucl. Mater. 189 (1992) 141.
[4] J. Rest, G.L. Hofman, J. Nucl. Mater. 210 (1994) 187.
[5] I.L.F. Ray, H. Thiele, Hj. Matzke, J. Nucl. Mater. 188 (1992) 90.
[6] K. Nogita, K. Une, Nucl. Instrum. Meth. B 91 (1994) 301.
[7] M.R. Hayns, J. Nucl. Mater. 56 (1975) 267.
[8] M.H. Yoo, J. Nucl. Mater. 68 (1977) 193.
[9] M.H. Yoo, J.O. Stiegler, J. Nucl. Mater. 69&70 (1978) 813.
[10] N.M. Ghoniem, J. Nucl. Mater. 89 (1980) 359.
[11] T. Hashimoto, in: N. H. Packan, R. E. Stoller, and A. S. Kumar (Eds.), Proc. On Effects of Radiation on Materials: 14th Int. Symp., ASTM STP 1046, vol. 1, American Society for Testing and Materials, Philadelphia, 1989, p. 523.
[12] J. Rest, J. Nucl. Mater. 207 (1993) 192.
[13] N. Hansen, D. Kuhlmann-Wilsdorf, Mater. Sci. Eng. 81 (1986) 141.
[14] A.B. Lidiard, J. Nucl. Mater. 19 (1966) 106.
[15] Hj. Matzke, Diffusion Processes in Nuclear Materials, R.P. Agarwala (Ed.), Elsevier, Amsterdam, 1992, p. 9.
[16] S.M. Murphy, J. Nucl. Mater. 168 (1989) 31.
[17] N.Q. Lam, S.J. Rothman, R. Sizmann, Radiat. Eff. 23 (1974) 53.
[18] W. Schilling, H. Ullmaier, in: B.R.T. Frost, (Ed.), Materials Science and Technology, Part ll, Chap. 9, vol. 10B, VCH, New York, 1994, p. 180.
[19] G. Duesing, H. Hemmerich, W. Sassin, W. Schilling, Int. Conf. on Vacancies and Interstitials in Metals, vol. 1, Jülich, Germany, 1968, p. 246.
[20] A.D. Whapham, B.E. Sheldon, Philos. Mag. 12 (1965) 1179.
[21] S. Kashibe, K. Une, K. Nogita, J. Nucl. Mater. 206 (1993) 22.
[22] J. Rest, J. Nucl. Mater. 120 (1984) 195.
[23] H. Assmann, R. Manzel, J. Nucl. Mater. 68 (1977) 360.
[24] I.L.F. Ray, personal communication, European Commission, Joint Research Center, Institute for Transuranium Elements, Karlsruhe, Germany, July, 1999.
[25] J. Rest, GRASS-SST: A Comprehensive Mechanistic Model for the Prediction of Fission-Gas Behavior in UO_2-base Fuels during Steady-State and Transient Conditions, NUREG/CR-0202, Argonne National Laboratory Report ANL-95/36 (1978).
[26] K. Nogita, K. Une, J. Nucl. Mater. 226 (1995) 302.
[27] G.L. Hofman, G.L. Copeland, J.E. Sanecke, Nucl. Tech. 72 (3) (1986) 338.
[28] L.E. Thomas, C.E. Beyer, L.A. Charlot, J. Nucl. Mater. 188 (1992) 80.
[29] D. Baron, B. Hermitte, J.P. Piron, in: Proc. IAEA Tech. Committee Meeting on Advances in Pellet Technology for Improved Performance at Hign Burn-up, Tokyo, Japan, 1996, Paper 3/7 (to be published).
[30] Hj. Matzke, Radiat. Effects 53 (1980) 219.